International Journal of Scientific Research in Science, Engineering and Technology

Print ISSN - 2395-1990
Online ISSN : 2394-4099

OPEN ACCESS

Available Online at :www.ijsrset.com
doi : https://doi.org/10.32628/IJSRSET2512505

Spectroscopical Investigation of Human Grown Urinary Calculi in and Around Puducherry Region

Vijayaprasath R[1], Selvaraju R[2], Renuka Devi K.B[3]

[1]Department of Physics, Manakula Vinayagar Institute of Technology, Puducherry, 605 107, India

[2]Engineering Physics, Faculty of Engineering and Technology, Annamalai University, Annamalainagar, 608 002, India

[3]Department of Physics, Rajiv Gandhi College of Engineering and Technology, Puducherry, 605 108, India

ARTICLEINFO

Article History:

Accepted: 05 June 2025
Published: 15 July 2025

Publication Issue :
Volume 12, Issue 4
July-August-2025
Page Number :
84-97

ABSTRACT

Urinary calculi taken from patients in the Southern Indian area of Pondicherry are spectroscopically analysed in this study. The chemical content, molecular structure and categorization of 20 urinary stone samples are ascertained by the use of complementary Ultraviolet – Visible (UV-Vis) and Fourier Transformer – Infrared (FTIR) spectroscopy methods. FT-IR analysis confirmed the presence of specific functional groups associated with Calcium oxalate, Calcium phosphate, Uric acid, Struvite and mixed composition. UV spectroscopy revealed distinctive absorption patterns between 200-400nm providing initial identification of stone type. According to the results the majority of the people under study had calcium oxalate (62%) followed by the uric acid (19%), calcium phosphate (11%), struvite (6%) and mixed composition (2%). A quick, accurate and non-destructive analytical tool for the clinical diagnosis and epidemiological evaluation of urolithiasis in the area is provided by this dual Spectroscopical technology. The Scanning Electron Microscopy (SEM) analysis shows the morphology of the collected samples. The result offer important information for creating treatment plans and targeted prevention measures tailored to the urolithiasis patterns seen in the Pondicherry community.

Keywords— Urolithiasis, Calcium oxalate, Uric acid, FT-IR, SEM

INTRODUCTION

A depressing chronic ailment that is becoming more prevalent worldwide is renal stone disease, often known as nephrolithiasis. Ever since the dawn of civilization, urolithiasis has been present in the

human race and is a major cause of morbidity and mortality worldwide [1].

Kidney stones are solid crystals that are created when minerals dissolved in urine. Common metabolic and environmental issues are the main causes of kidney stones. Men are more likely to be affected then that woman to have kidney stones. The exact cause of this condition is unknown but it has been linked to a number of factors including lifestyle choices, diet, animal protein, hot weather, low water intake, geographic factors like climate changes and higher rates of diabetes, obesity, hypertension, hypotension, gender, age and food habits that raise the risk of nephrolithiasis and stone formation [2,4].

About 10% of people in developed and industrialized nations have been known to have it at some point in their lives. The lifetime risk of renal stones ranges from 10% to 15% in the USA, from 1% to 5% in Asia, and from 5% to 9% in Europe. Due to varying risk factors in the populations, the frequency of different stone types also differs throughout nations. Although Tamilnadu and Pondicherry are not in the urinary stone belt, kidney stones are predicted to affect 12% of people in tropical and semi - arid areas of India.[3].

The size of kidney stones can vary from millimeters to centimeters. Many develop and are undetectable through urine, but stones larger than 3 mm can block the ureter, leading to muscular spasms, severe episodic lower abdomen and flank pain and dilation of the upper ureter and renal pelvis. Pain concentration usually varies from patient to patient and is correlated with stone size and surface roughness. Because of the roughly 50% chance of recurrence, stones bigger than 10 mm typically require surgical removal followed by preventive treatment based on the chemical makeup of the stone [5].

Numerous organic and inorganic components contribute to the production of urinary stones, which vary in chemical composition and are unique to each patient. Most stones fall into one of five categories. Stones made of calcium oxalate and calcium phosphate combine to form the majority of kidney stones [6]. Because adenine, xanthine and uric acid precipitate under low urine pH conditions, patients develop uric acid stones, which are crystallized mixtures of uric acid [7]. Magnesium phosphate stones, also known struvite are classified as infectious stones because they develop when alkaline urine containing urease producing bacteria contains high levels of ammonium and trivalent phosphate [8].

Cysteine leakage into the urine results in cysteine stones. A higher risk of stone recurrence is identified in patients with cystinuria [9]. To comprehend how kidney stones originate, it is crucial to investigate their chemical makeup. In order to properly manage kidney stone disease and avoid its recurrence, the medical therapy that is chosen for the condition is often determined by a study of the stones [10].

Urine typically has a pH of 6.0, which is mildly acidic, however it can vary from 4.5 to 8.0. Numerous illnesses have been linked to the pH of the urine. Furthermore, it has been noted that the pH of the urine can alter the levels of numerous forms of stones, such as calcium oxalate, calcium phosphate and uric acid. Urine with an acidic pH is linked to cysteine and uric acid stones, whereas urine with a basic pH is more likely to generate phosphate containing stones [12].

Numerous analytical techniques have been develop as a result of the varied composition of urinary calculi. Rapid stone categorization based on absorption patterns is made possible by ultraviolet-visible spectroscopy, especially for calcium oxalate hydrates and uric acid variations. It identifies the quantities of mixed elements for treatment monitoring, connects spectral signatures with metabolites and links spectral patterns to clinical indicators. Without the need for solvents, Fourier Transform Infrared (FTIR) spectroscopy offers a qualitative and semi-quantitative examination of kidney stone composition. By analysing distinctive infrared

absorption patterns depending on chemical bonding and structure this method identifies ingredients. When infrared radiation is passed through powdered stone samples that have been crushed with potassium bromide into a transparent wafer, signature spectrum scans are produced by oscillations in the molecules and crystals.

In this present study human- grow kidney stones are obtained, the mineral composition and morphology is assessed by using FT-IR, UV-visible spectroscopy and Scanning Electron Microscopy techniques. Fourier Transform Infrared Spectroscopy (FTIR) used to analyse Kidney stones using a Thermo Nicolet 6700 device set up to scan form 5000 to 50cm^{-1} at 0.1cm^{-1} resolution. Standard procedures were followed during the preparation of the samples. A 13mm diameter disc was formed by compression after the stone materials were mixed with moisture free potassium bromide in a 10:1 ratio. A highly adaptable device with a high resolution of 0.1nm, the SHIMADZU UV-Vis –NIR spectrometer, model 3600 is made for thorough spectroscopic examination over a wide wavelength range of 175nm to 1000nm. Usually needing 0.5g top 1g of fine powder, this sophisticated system is well suited for studying powder samples is perfect for thoroughly characterizing material according to their absorption and reflection characteristics in the visible, near infrared and ultraviolet spectrum. Scanning Electron Microscopy JEOL-JSM-IT200 with the magnification of x 18 TO 30,000 and a resolution of 3.0nm (HV), 4.5nm (LV) with the accelerating voltage of 0.5Kv to 30Kv calibrate to study the morphological, topographical and compositional information about the surface of the kidney stones.

MATERIALS AND METHOD

1.1 CLINICAL SURVERY ON UROLITHIASIS PATIENTS AND STONE COLLECTION

Kidney stones are collected using fine strainers or special collection devices when patients urinated. After collection, the stones were tenderly washed with distilled water to remove any biological material while keep the stones intact. The stones were then completely air-dried at room temperature avoiding the use of heat which could change their composition.

The stones were put in sterile containers (plastic vials or specimen containers) once they had dried. Filtered sheets are used for extremely tiny stones. Patient's identification the date of collection and other clinical characteristics are meticulously noted on each sample. Chemicals and preservatives are not added to the stones since they might obstruct a precise examination total 20 samples were collected and the findings are processed using Microsoft Excel and presented in graphical format.

Fig.1 Collected Urinary stones (UR01-UR20)

RESULTS AND DISCUSSION

2.1 FOURIER TRANSFORM INFRARED ANALYSIS OF URINARY STONES

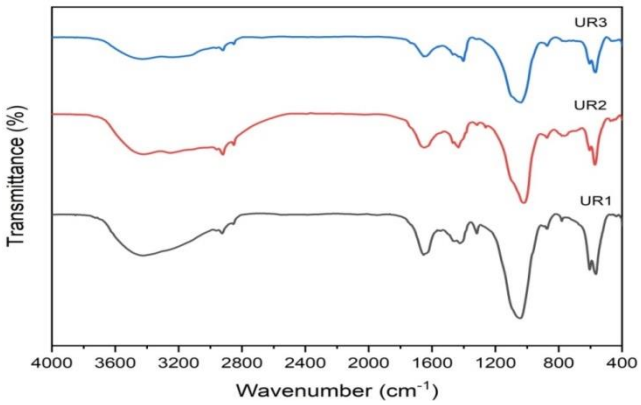

FIG.2. The FT-IR spectra of urinary stones (UR1-UR3)

TABLE 1. FT-IR Spectral data of urinary stones (UR1-UR3)

Wavenumber (cm^{-1})			Tentative assignments
UR1	UR2	UR3	
3424	3421	3425	O-H stretching vibration
2925	2920	2920	C-H stretching vibration
2847	2851	2856	C-H symmetric stretching vibration
1653	1651	1652	C=O stretching vibration
1421	1433	1402	PO_4 group stretching vibration
1317	-	-	C-O stretching vibration
1041	1018	1039	PO_4^{3-} group stretching vibration
874	874	873	PO_4^{3-} group stretching vibration
780	779	-	C-C stretching vibration
604	604	605	PO_4^{3-} bending vibration
566	571	568	PO_4^{3-} bending vibration

FT-IR spectroscopic analysis of urinary stone samples Fig.2 (UR1, UR2 and UR3) revealed distinct absorption bands characteristics of functional groups associated with calcium oxalate. Broad peaks observed around 3424, 3421 and 3425 cm^{-1} in all three samples are attributed to O-H stretching vibrations, indicating the presence of hydroxyl groups commonly found in calcium oxalate given in table.1 [13]. Bands in the range of 2920 – 2925 cm^{-1} correspond to asymmetric C-H stretching, while a weaker symmetric C-H stretching bands are noted at 2851 cm^{-1} in sample UR2 [14]. A strong absorption band observed between 1651 – 1653 cm^{-1} is assigned to C=O stretching vibrations, a key indicator of oxalate [15].

Multiple C-O stretching bands found in the 1402 – 1433 cm^{-1}, 1317 cm^{-1} in UR1 and in between 1018-1041cm^{-1} area provide additional evidence of the oxalate structure. Furthermore, calcium oxalates monohydrate – specific C-C stretching vibrations are detected between 873 – 874 cm^{-1} and 779 – 780 cm^{-1}. The carboxylate group's (O-C=O) bending vibrations are seen in the band in the 566 -605 cm^{-1} [16].

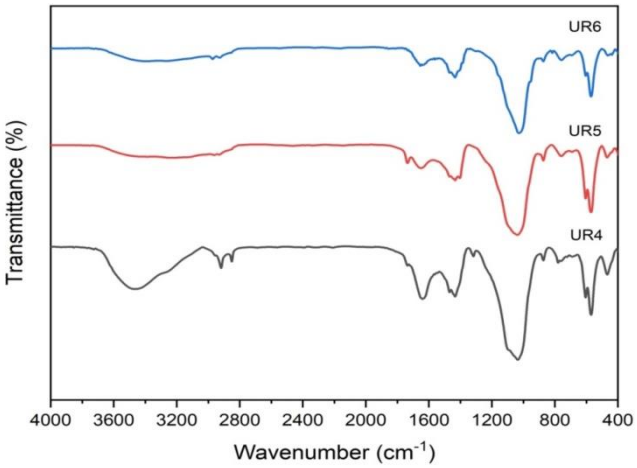

FIG.3 The FT-IR spectra of urinary stones (UR4-UR6)

TABLE 2. FT-IR Spectral data of urinary stones (UR4-UR6)

Wavenumber (cm^{-1})			Tentative assignments
UR4	UR5	UR6	
3463	-	-	O-H stretching
-	-	3385	O-H stretching
-	3240	-	O-H stretching
2918	-	2900	C-H asymmetric stretching
2850	-	2840	C-H symmetric stretching
-	1735	-	C=O stretching
1640	1648	1653	C=O stretching
1433	1432	1434	Po_4group stretching
1035	1037	1028	PO_4^{3-} bending vibration
873	873	-	C-C stretching
779	758	758	C-C stretching
605	605	604	PO_4^{3-} bending vibration
570	570	570	PO_4^{3-} bending vibration
467	469	464	Ring deformation

The multiple distinctive absorption bands from the Fig.3 samples (UR4, UR5 and UR6) that are suggestive of calcium oxalate and its monohydrate form and calcium posphate. At around 3463 cm^{-1} in UR4, 3385 cm^{-1} in UR6 and 3240 cm^{-1} in UR5, significant O-H

stretching vibrations are found, indicating the presence of hydroxyl groups given in table 2. Additionally, C-H stretching bands at 2918 cm^{-1} and 2850 cm^{-1} in UR4 provided evidence of the presence of organic components inside the calcium oxalate matrix [17].

Strong C=O stretching related absorption bands in the 1640 – 1653 cm^{-1} region are seen in all samples and UR5 also showed an extra peak at 1735 cm^{-1}. Consistent C-O stretching vibrations are detected at around 1432 – 1434 cm^{-1} and 1028 – 1037 cm^{-1}. C-C stretching bands between 758 and 779 cm^{-1} and at 873 cm^{-1} (UR4 and UR5) verified the existence of calcium oxalate monohydrate. The presence of low – frequency bending vibrations linked to the carboxylate (O-C=O) and ether like (O-C-O) groups are further supported by the observation of these vibrations at 604 – 605 cm^{-1}, 570 cm^{-1} and between 464 – 469 cm^{-1} [18].

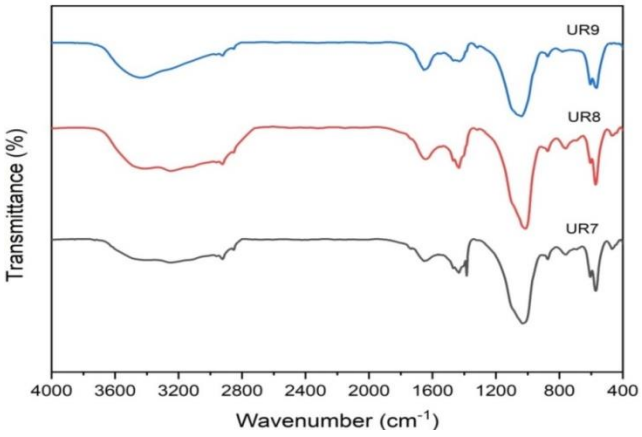

FIG.4 The FT-IR spectra of urinary stones (UR7-UR9)

The FT-IR spectra shown in Fig .4 are UR7, UR8 and UR9. Different absorption bands that are consistent with calcium oxalate are visible in the spectra. A noticeable broad band that corresponded to O-H stretching vibrations and verified the presence of hydroxyl groups is seen in UR9 at about 3439 cm^{-1} and in UR7 and UR8 in between 3249 and 3250 cm^{-1}. Asymmetric C-H stretching is identified as the cause of the peaks at 2922 cm^{-1} [19]. In UR7 and UR9 the C=O stretching vibration a crucial indicator of oxalate occurred regularly at 1653 cm^{-1}, whereas in UR8, it slightly shifted to 1640 cm^{-1}. All three samples are noticeable C-O stretching vibrations, especially in the 1432 -1433 cm^{-1}region. There are also peaks at 1385 cm^{-1} and in the 1031 – 1039 cm^{-1} range.

The calcium oxalate monohydrate specific C-C stretching vibrations are detected at 873 $cm^{-1}$and in the range of 759 – 760 cm^{-1} [20]. The O-C=O group exhibited bending vibrations at 605, 604 and 571 cm^{-1} with UR9 exhibiting a noticeable band at 566 cm^{-1}. The tentative assessment of the wavenumbers in given in table 3. All together these spectral characteristics verify that the main constituent of the examined stone samples is calcium oxalate, especially in its hydrated state [21].

TABLE 3. FT-IR Spectral data of urinary stones (UR7-UR9)

Wavenumber(cm^{-1})			Tentative assignments
UR7	UR8	UR9	
3424	3428	3439	O-H stretching vibration
3249	3250	-	O-H stretching vibration
2922	2910	2908	C-H asymmetric stretching vibration
1653	1640	1653	O-H deformation vibration
1433	1433	1432	Po_4^{3-} group vibration
1385	-	-	C-C of vibration
1031	1013	1039	PO_4^{3-} stretching vibration
873	873	873	C-C stretching vibration
759	760	-	PO_4^{3-} stretching vibration
605	604	604	PO_4^{3-} bending vibration
-	554	566	PO_4^{3-} bending vibration
571	571	-	PO_4^{3-} stretching vibration
467	469	-	Ring deformation

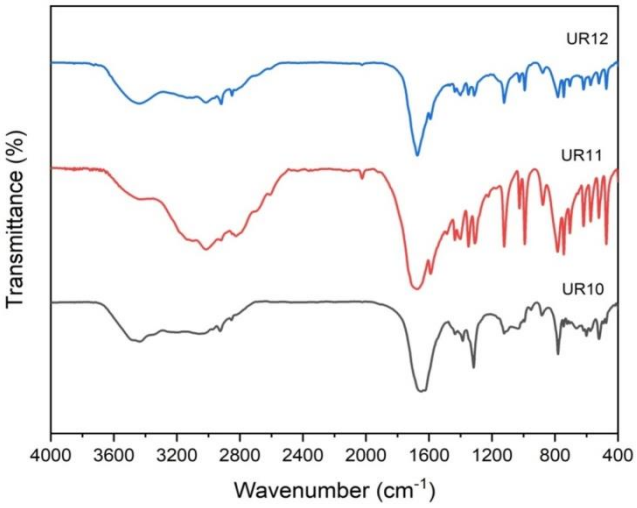

FIG.5 The FT-IR spectra of urinary stones (UR10-UR12)

The uric acid specific absorption bands are seen inn Fig.5 the stone samples UR10, UR11 and UR12. Significant N-H stretching band are seen at 3059 cm^{-1} in UR10 and prominent O-H stretching vibrations are found at 3435 cm^{-1}in UR10 and 3436 cm^{-1} in UR12 at 3014 cm^{-1} in UR11 and 3015 cm^{-1} in UR12 C-H stretching vibrations are detected. In the 2925-2850 cm^{-1} range, symmetric and asymmetric C-H stretching bans are found. In UR11 a combination band is detected at 2024 cm^{-1}. All three samples consistently exhibited strong C=O stretching vibrations between 1648 and 1674cm^{-1}, which are a sign of uric acid [22].

The mid and low frequency sections of the spectra showed additional absorption bands that corresponded to C=C stretching, C-N stretching and ring deformation vibrations. These spectrum characteristics verify that the main component of the samples UR10, UR11 and UR12 is uric acid.

TABLE 4. FT-IR Spectral data of urinary stones (UR10-UR12)

Wavnumber (cm^{-1})			Tentative assignments
UR10	UR11	UR12	
3435	-	3436	N-H stretching Vibration
3059	3054	3052	O-H stretching Vibration
-	3014	3015	O-H stretching Vibration
2925	-	2918	C-H asymmetric stretching Vibration
-	2825	2850	C-H symmetric stretching Vibration
1648	1674	1673	C=O stretching Vibration
-	1589	1591	C=C stretching Vibration
-	1401	1400	C-N stretching Vibration
1385	1372	1378	C-C stretching Vibration
-	1349	1349	C-N stretching Vibration
1316	1309	1312	C-N stretching Vibration
-	1026	1026	C-N stretching Vibration
883	877	877	C-C Stretching Vibration
-	744	744	PO_4^{3-} stretching Vibration
781	705	706	PO_4^{3-} stretching Vibration
600	618	618	PO_4^{3-} bending Vibration
-	573	574	PO_4^{3-} stretching Vibration
521	521	521	O-C-O in plane bending Vibration
475	474	474	Ring deformation

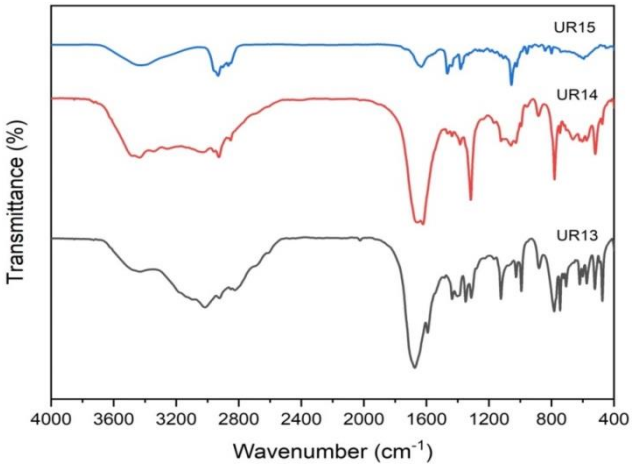

FIG.6 The FT-IR spectra of urinary stones (UR13-UR15)

Different absorption bands that molecular structures and functional groups mostly associated with uric acid were visible in the resulting spectra of the three samples (UR13, UR14 and UR15). The existence of noticeable O-H stretching vibrations at 3435 cm^{-1} in UR14 and 3423 cm^{-1} in UR15 indicates the presence of uric. In UR14 and UR15 asymmetric and symmetric C-H stretching vibrations that are also linked to uric acid are found in the 2927-2866 cm^{-1} range whereas in UR13, C-H stretching is found at 3015 cm^{-1}. UR13 at 1674 cm^{-1} andUR14 and UR15 between1621 and 1632 cm^{-1} have characteristic carbonyl (C=O) stretching bands which demonstrates the existence of uric acid.

The resultant spectra of the three tone samples (UR13, UR14 and UR15) show distinct absorption bands that correspond to molecular structures and functional groups largely associated with uric acid shown in Fig.6. Uric acid is indicated by notable O-H stretching vibrations at 3435cm^{-1} in UR14 and 3426 cm^{-1} in UR15 [23].

TABLE 5. FT-IR Spectral data of urinary stones (UR13-UR15)

Wavenumber (cm^{-1})			Tentative assignments
UR13	UR14	UR15	
-	3435	3423	N-H stretching Vibration
3015	3012	3015	C-H stretching Vibration
-	2927	2932	C-H asymmetric stretching Vibration
1674	1670	1672	C=O stretching Vibration
-	1621	1632	C=O stretching Vibration
1591	1585	1584	C=C stretching Vibration
1466	-	1466	C-N stretching Vibration
1435	1436	-	C-N stretching Vibration
-	1384	1381	C-N stretching Vibration
1313	1316	-	C-N stretching Vibration
1191	1186	1191	C-O stretching Vibration
1123	-	1108	N-H bending Vibration
-	1058	1056	C-O stretching Vibration
992	986	990	C-O stretching Vibration
879	883	840	C-H out-of-plane bending Vibration
782	780	799	C-C stretching Vibration
723	-	720	Ring deformation Vibration
706	-	708	Ring deformation Vibration
522	520	-	O-C-O in plane bending
474	475	-	Ring deformation

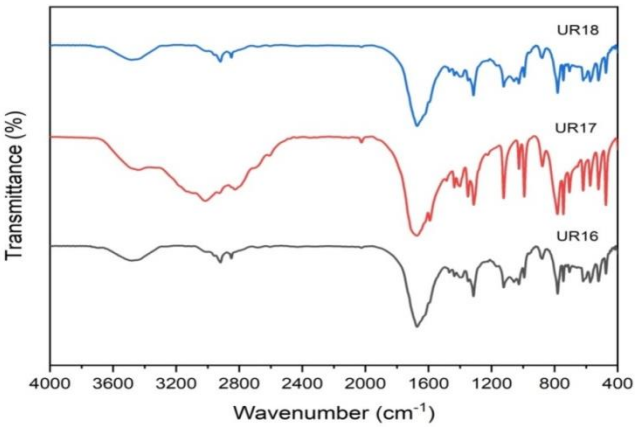

FIG.7 The FT-IR spectra of urinary stones (UR16-UR18)

TABLE 6. FT-IR Spectral data of urinary stones (UR16-UR18)

Wavenumber (cm-1)			Tentative assignments
UR16	UR17	UR18	
3482	-	3482	N-H Stretching vibration
-	3014	-	O-H stretching vibration
2919	-	2919	C-H asymmetric stretching vibration
2850	2826	2850	C-H symmetric stretching vibration
1670	1673	1672	C=O stretching vibration
1583	1591	1585	C=C stretching vibration
1400	1401	1400	C-N stretching vibration
1399	-	1399	C-C of vibration

Wavenumber (cm-1)			Tentative assignments
UR16	UR17	UR18	
1314	1313	1314	Vibration of C-O
-	1236	1234	C-N stretching vibration
1122	1123	1122	N-H bending vibration
992	992	992	Ring deformation vibration
878	877	878	C-H out-of-plane bending vibration
780	782	780	C-C stretching vibration
744	744	744	PO_4^{3-} group vibration
706	706	706	Ring deformation vibration
618	619	618	Ring deformation vibration
573	574	573	Ring deformation vibration
521	522	521	O-C-O in plane bending vibration
474	475	474	NH^{+}_{4} deformation vibration

Urinary stone samples from (UR16, UR17 and UR18) were analyzed using FT-IR spectroscopy which produced distinctive absorption frequencies shown in Fig.7 that allowed for the identification of several minerals components. The existence of hydrated phases is indicated by the large absorption bands seen at 3482 cm^{-1} and 3014 cm^{-1} which correspond to O-H stretching vibrations. Asymmetric and symmetric modes at 2917 cm^{-1} and 2850-2826 cm^{-1}respectively were used to identify the C-H stretching vibrations which are characteristic of calcium oxalate monohydrate (COM). Distinct peaks at 1670-1673 cm^{-1} (C=O stretching), 1583 – 1591 cm^{-1} (C=C stretching) and 1400 – 1401 cm^{-1} (C-N stretching) verified the existence of uric acid (uricite). Using N-H bending peaks at 1122-1123 cm^{-1}, ring deformation at 992 cm^{-1} , C-H out of plane being at 878 - 877 cm^{-1} ring deformation at 706 cm^{-1} and NH_4^+ deformation at 474 – 475 cm^{-1} provided additional proof of uric acid [24].

Ring stretching and vibration modes at 1057 cm^{-1}, 1026 cm^{-1}, 618-619 cm^{-1} and 573-574 cm^{-1} while Uric acid displayed distinctive bands at 1435 – 1436 cm^{-1} and 744 cm^{-1}. Specific vibrational modes such as C-C stretching at 780-782 cm^{-1}, C-O stretching at 1313 – 1314 cm^{-1}, O-C-O in-plane bending at 521 – 522 cm^{-1} and C-C vibration at 1399 cm^{-1} [25]. These spectroscopic results show that the urinary stones have a complicated mineralogical composition with calcium oxalate monohydrate, uric acid and different phosphate minerals being the main phases.

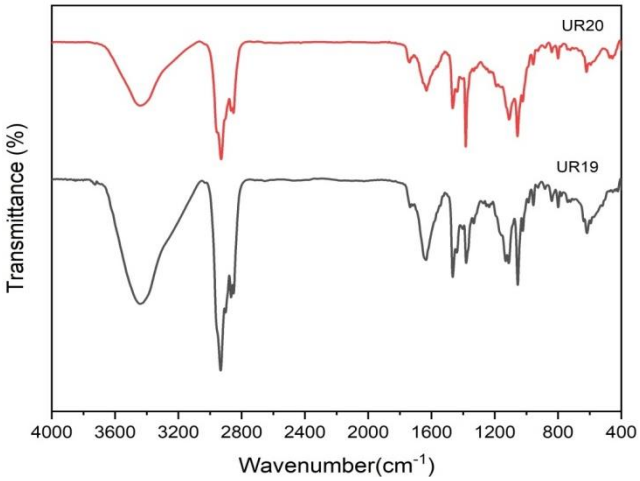

FIG.8 The FT-IR spectra of urinary stones (UR19-UR20)

Heterogeneous Mineral compositions are consistent with the unique absorption patterns seen in the FT-IR spectroscopic analysis of urine stone samples from (UR19 and UR20) shown in fig 8. The O-H stretching vibrations found at 3442-3441 cm^{-1} shown that hydrated calcium oxalate phases were present. To identify calcium oxalate monohydrate (COM) a number of distinctive peaks were employed including C-C asymmetric stretching at 2932-2929 cm^{-1}, C-H symmetric stretching at 2866-2851 cm^{-1} and a distinctive C=O stretching band t 1738 cm^{-1} in sample UR20. Other COM – specific vibrations were found to be C-C stretching at 799 cm^{-1}, C-H out-of-plane bending at 956-957 cm^{-1} and 839 cm^{-1} and C-C vibration at 1380-1383 cm^{-1}.

C-C stretching vibrations at 1633-1631 cm^{-1}, N-H bending at 1111-1109 cm^{-1} and NH_4^+ deformation at 456 cm^{-1} in sample UR20 were used to prove the existence of uric acid. The tentative assessment of the

spectra is given in table 7. Multiple ring deformation and stretching modes at 1054-1056 cm^{-1}, 1022-1023 cm^{-1} and 617 – 620 cm^{-1} demonstrated the existence of hydroxyapatite [26]. A complex multi- component mineralogical composition typical of mixed urinary calculi is indicated by the spectroscopic data which shows urinary stones are primarily composed of calcium oxalate monohydrate with notable contributions from uric acid, calcium carbonate and hydroxyapatite phases.

TABLE 7. FT-IR Spectral data of urinary stones (UR19-UR20)

Wavenumber (cm^{-1})		**Tentative assignments**
UR19	**UR20**	
3442	3441	O-H stretching vibration
2932	2929	C-C asymmetric stretching vibration
2866	2851	C-H symmetric stretching vibration
-	1738	C=O stretching vibration
1633	1631	C=C stretching vibration
1465	1466	C-C stretching vibration
1380	1383	C-C stretching vibration
1111	1109	N-H bending vibration
1054	1056	Ring deformation
1022	1023	PO_4^{3-} stretching vibration
956	957	C-H out-of-plane bending vibration
839	839	C-H out-of-plane bending vibration
799	799	C-C stretching vibration
617	620	Ring deformation
-	456	NH^{+}_4 deformation

2.2 UV-VISIBLE ANALYSIS OF URINARY STONES

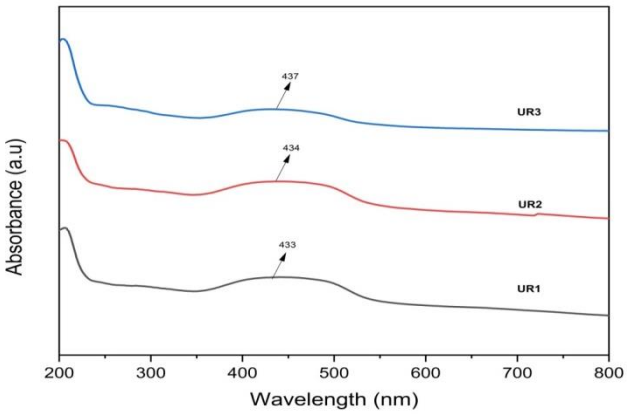

FIG.9. The UV-Visible spectra of urinary stones (UR1-UR3)

The distinct samples (UR1, UR2 and UR3) and their absorption spectra from UV- visible spectroscopy are shown in the fig.9. The wavelength range from 200 to 800nm, covering both the visible (400 – 800nm) and ultraviolet (200- 400nm) ranges. In the visible spectrum, each sample shows a distinctive absorption maximum in the blue - violet region. Specifically at λ_1 = 433nm, λ_2 = 434nm and λ_3 = 437nm [27] respectively.

These peaks show that light absorption in this specific region of the visible spectrum is the strongest for all three samples. The three samples exhibit comparable spectral patterns, but their absorption intensities and maximum wavelength vary slightly. The electronic transitions within the molecules specifically $\pi \rightarrow \pi^*$ or $n \rightarrow \pi^*$transitions, are probably the cause of the observed absorption maxima about 400 – 450nm confirms the presence of hydroxyl and carbonyl compound.

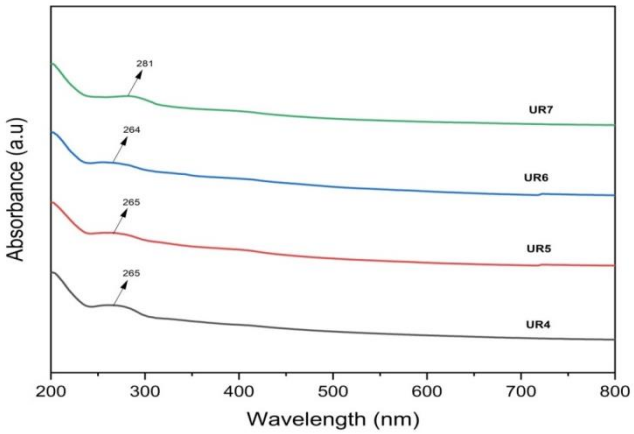

FIG.10. The UV-Visible spectra of urinary stones (UR4-UR7)

UR4, UR5, UR6 and UR7 exhibiting prominent absorption maxima in the UV band between 200 and 300 nm appear in the absorption spectra shown in Fig 10. Strong UV activity is evident in all of these samples, which exhibit distinctive peaks at λ_4 = 265nm, λ_5 = 265nm, λ_6 = 264nm and $\lambda 7$ = 281nm [28] respectively. The four samples exhibit comparable spectral signatures but vary in their absorption intensities. The 200 – 300 nm range of detected absorption bands typically corresponds to n → π* electronics transitions that are occurring within the samples.

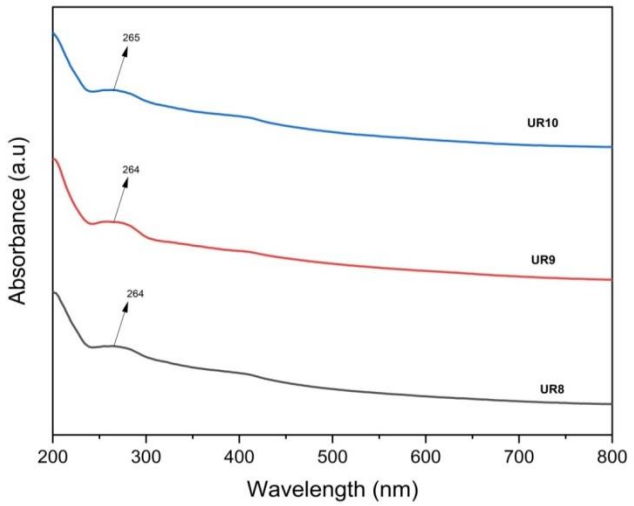

FIG.11. The UV-Visible spectra of urinary stones (UR8-UR10)

Each spectra in Figure.11 has a characteristic absorption peak at 200 – 300 nm, labeled λ_8 = 264nm, λ_9 = 264nm, and λ_{10} = 264nm [29]. This suggests that all three samples absorb light most strongly when it is UV active. Higher absorbance is shown in the UV area of all three spectra, which progressively decreases as wavelength increases toward the visible spectrum's red end. Similar spectral are displayed by the three samples (UR8, UR9 and UR10), however their intensities and modest variations in their absorption maxima indicate that they may be related compounds or the same chemical under various circumstances. Then n → π* electronics transitions in the molecules under study are probably represented by the particular peaks at 200 – 300 nm.

The four samples (UR11, UR12, UR13 and UR14) with unique absorption maxima in the 200 – 300 nm Ultra violet regions are shown in Figure.12 along with their absorption spectra. These compounds absorb photons most efficiently in the UV area, as seen by the particular peaks at λ_{11} = 251nm, λ_{12} = 261nm, λ_{13} = 259nm and λ_{14} = 259nm [30]. As wavelengths move toward the longer, red end of the visible spectrum, there is a constant pattern of absorption strength progressively decreasing with all four spectral profiles exhibiting their maximum absorbance values in the UV. These samples appear to be structurally related chemical entities possibly the same compounds that were examined under various experimental settings, based on the observed spectrum similarities between them. Usually the absorption bands that show up in the 200 – 300 nm region are associated with n → π* electronics transitions that take place in the molecular structures under investigation.

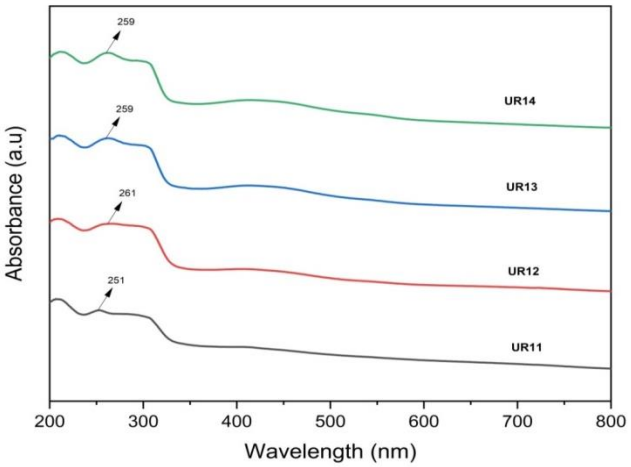

FIG.12. The UV-Visible spectra of urinary stones (UR11-UR14)

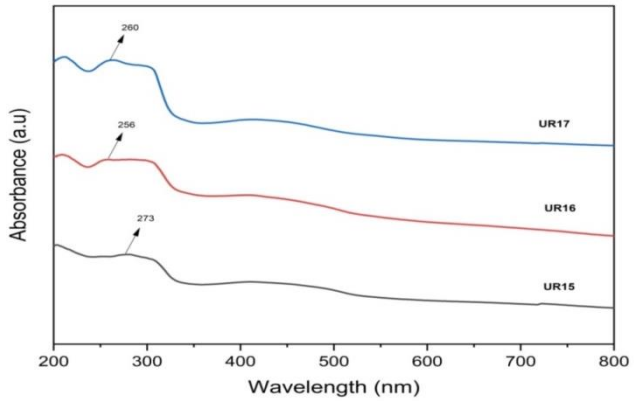

FIG.13. The UV-Visible spectra of urinary stones (UR15-UR17)

Each spectra in Figure.13 includes a specific absorption peak at 200-300 nm, marked lables λ15 = 273nm, λ_{16} = 256nm and λ_{17} = 260nm [30]. This suggests that all three substances absorb light most effectively when it is UV active. Higher absorbance is shown in the UV area of all three spectra, which spectra which progressively decrease as wavelength increase toward the visible spectrum red end. Similar patterns are displayed by the three samples (UR15, UR16 and UR17) however their intensities and modest variations in their absorption maxima indicate they may be related compounds or the same molecule under various circumstances. The n → π* electronic transitions in the molecules under study are probably expressed in the particular peak at 200 – 300nm.

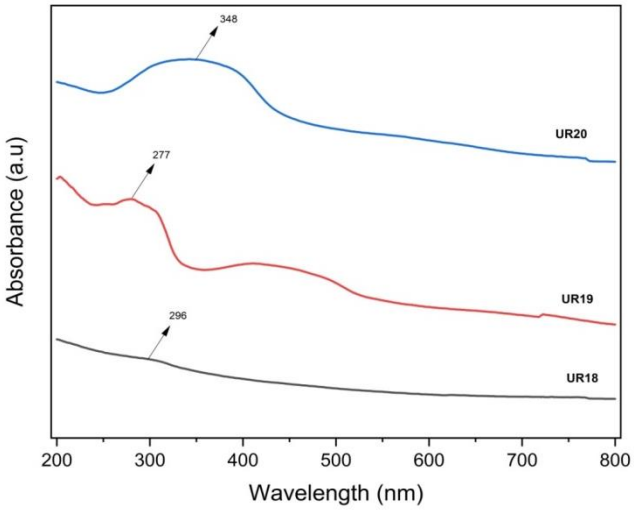

FIG.14. The UV-Visible spectra of urinary stones (UR18-UR20)

The samples UR18, UR19 and UR20 with distinctive absorption maxima in the UV band between 200 and 350 nm are shown in the absorption spectra in figure 14. These samples exhibit high light absorption in the UV spectrum with notable peaks at λ_{18} = 296nm, λ_{19} = 277nm and λ_{20} = 348nm [28,31] respectively. The 200 – 350nm range of detected absorption bands usually corresponds to n → π* electronic transitions that take place inside the molecular structures.

UV-Visible spectroscopies for all the collected samples are carried out (UR01-UR20). The presence of absorption peak between 200-400nm confirms that the samples are UV active due to the presence of carbonyl and hydroxyl compound present in the sample.

2.3 SCANNING ELECTRON MICROSCOPY ANALYSIS OF URINARY STONE

The comparative analysis of samples UR1 through UR20 shown in **Fig.15** reveals remarkable diversity in kidney stone morphology, reflecting the complex interplay of physiological, metabolic, and environmental factors during stone formation. The SEM analysis of sample reveals a heterogeneous crystalline structure characterized by irregular aggregates distributed across the stone surface. The

morphology displays a distinctive combination of both fine-grained and coarse crystalline domains, with crystal faces appearing well-defined and exhibiting sharp edges typical of organized mineral formation. This organized crystal growth pattern suggests a more controlled formation environment compared to other samples, indicating potentially different physiological conditions during stone development.

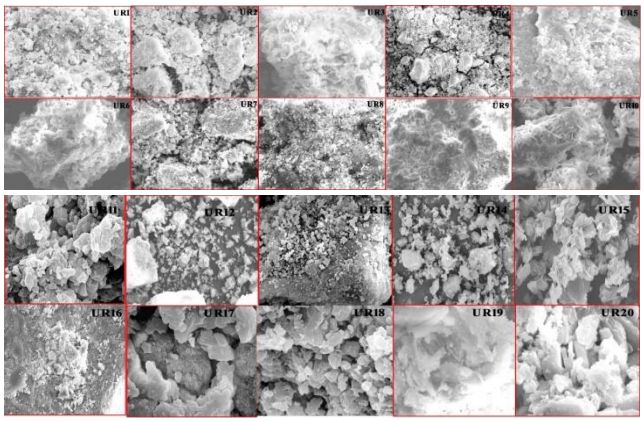

Fig 15. Scanning electron micrograph of UR01 – UR20

CONCLUSION

The combined UV-visible and FT-IR spectroscopic characterisation is a very useful method for through urine stone analysis in the Pondicherry area. This approach offers a useful foundation for clinical diagnosis, treatment planning and prevention tactics in addition to advancing our knowledge of local urolithiasis trends. The findings give important information for medical professions creating region specific kidney stone management strategies, which will ultimately lead to better patient outcomes and a lower disease burden in the population under study. This dual spectroscopic technique's successful application shows that it has the potential to be used more widely in clinical settings. It offers a dependable, effective and economical solution for urinary stone characterisation that can greatly improve the standard of care for urolithiasis in both clinical and research context. The initial exploration of UV-Visible spectroscopy of the human grown urinary stone is performed in this study. This distinctive morphology may indicate a highly porous, sponge-like architecture with numerous interconnected cavities and channels visible throughout the surface. The surface texture appears notably rough and irregular, with crystal formation showing a less organized pattern when compared to the more structured samples.

Acknowledgement

I thank Centralized Instrumentation and Service Laboratory (CISL), Department of Physics, Annamalai University helping for analyzing Scanning Electron Microscopy.

REFERENCES

[1]. Selvaraju, R., Raja, A., & Thiruppathi, G. (2013). Chemical composition and binary mixture of human urinary stones using FT-Raman spectroscopy method. Spectrochimica Acta Part A: Molecular and Biomolecular Spectroscopy, 114, 650-657.

[2]. Selvaraju, R., Raja, A., & Thiruppathi, G. (2012). FT-Raman spectral analysis of human urinary stones. Spectrochimica Acta Part A: Molecular and Biomolecular Spectroscopy, 99, 205-210.

[3]. Sunitha, J., Thironavukkaras, P., & Ash, S. (2018). A retrospective study on prevalence and risk factors associated with kidney stone in Vellore district, Tamil Nadn. Int. J. Pharm. Sci. Rev. Res, 48(1), 54-57.

[4]. Dongre, A. R., Rajalakshmi, M., Deshmukh, P. R., Thirunavukarasu, M. R., & Kumar, R. (2017). Risk Factors for Kidney Stones in Rural Puducherry: Case-Control Study. Journal of clinical and diagnostic research : JCDR, 11(9), LC01–LC05.

[5]. Wang, X., Zhang, J., Ma, Z., Yang, Y., Dang, Y., Cao, S., ... & Hu, X. (2023). Association and interactions between mixed exposure to trace elements and the prevalence of kidney stones: a

study of NHANES 2017–2018. Frontiers in Public Health, 11, 1251637.

[6]. Selvaraju, R., & Bhuvaneswari, M. (2020). Growth and Spectral Investigation on Pure Calcium Phosphate Doped With (Copper and Magnesium) Crystals.

[7]. Vasuki, G., & Selvaraju, R. (2014). Growth and characterization of uric acid crystals. International Journal of Science and Research, 3(8), 696-699.

[8]. Selvaraju, R., & Sivasakthi, A. Spectral and Dissolution Studies on Pure Struvite with Nickel-Doped Struvite Crystals.

[9]. Hughes, T., Tzelves, L., & Somani, B. K. (2023). Cystine stones: developments in minimally invasive surgery and their impact on Morbidity and Stone Clearance. Research and Reports in Urology, 175-185.

[10]. Singh, V. K., & Rai, P. K. (2014). Kidney stone analysis techniques and the role of major and trace elements on their pathogenesis: A review. Biophysical Reviews, 6, 291–310.

[11]. Rimer, J. D., Kolbach-Mandel, A. M., Ward, M. D., & Wesson, J. A. (2017). The role of macromolecules in the formation of kidney stones. Urolithiasis, 45(1), 57-74.

[12]. Manissorn, J., Fong-Ngern, K., Peerapen, P., & Thongboonkerd, V. (2017). Systematic evaluation for effects of urine pH on calcium oxalate crystallization, crystal-cell adhesion and internalization into renal tubular cells. Scientific reports, 7(1), 1798.

[13]. Wregg, C., Rosenlechner, D., Zach, V., Eigenfeld, M., Stabentheiner, E., Ahyai, S., & Schwaminger, S. P. (2024). FT-IR Spectroscopy Analysis of Kidney Stone Variability in Styria. Crystals, 14(10), 854.

[14]. Basiri, A., Tahvildari, A., Naji, M., Ziaeefar, P., & Kashi, A. H. (2025). Determination of the kidney stone composition using infrared spectroscopy in Iran at a national referral center during 2019–2023. Asian Journal of Urology, 12(1), 72-78.

[15]. Zhang, J., Li, K., Chen, H., Hu, X., Guo, Z., Chen, S., ... & Chen, P. (2023). Retrospective analysis of urinary tract stone composition in a Chinese ethnic minority colony based on Fourier transform infrared spectroscopy. Scientific Reports, 13(1), 13453.

[16]. Maruyama, M., Sawada, K. P., Tanaka, Y., Okada, A., Momma, K., Nakamura, M., ... & Mori, Y. (2023). Quantitative analysis of calcium oxalate monohydrate and dihydrate for elucidating the formation mechanism of calcium oxalate kidney stones. PLoS One, 18(3), e0282743.

[17]. H. Valido, I., Resina-Gallego, M., Yousef, I., Luque-Gálvez, M. P., Valiente, M., & López-Mesas, M. (2020). Calcium oxalate kidney stones, where is the organic matter?: A synchrotron based infrared microspectroscopy study. Journal of Biophotonics, 13(12), e202000303.

[18]. Maruyama, M., Sawada, K. P., Tanaka, Y., Okada, A., Momma, K., Nakamura, M., ... & Mori, Y. (2023). Quantitative analysis of calcium oxalate monohydrate and dihydrate for elucidating the formation mechanism of calcium oxalate kidney stones. PLoS One, 18(3), e0282743.

[19]. Durdağı, S. E. V. İ. L. (2024). Urinary Stone Composition Analyses Using Fourier Transform Infrared (FTIR) Spectrometry. Journal of Urology and Renal Diseases, 9(04).

[20]. Gadzhiev, N., Gelig, V., Rodionov, G., Gauhar, V., & Zeng, G. (2025). Metabolic Differences in 24-Hour Urine Parameters Between Calcium Oxalate Monohydrate and Dihydrate Kidney Stones: A Clinical Study. Diagnostics, 15(8), 994.

[21]. Werner, H., Bapat, S., Schobesberger, M., Segets, D., & Schwaminger, S. P. (2021). Calcium oxalate crystallization: Influence of pH, energy input, and supersaturation ratio on the synthesis of artificial kidney stones. ACS omega, 6(40), 26566-26574.

[22]. Xu, S., Liu, Z. L., Zhang, T. W., Li, B., Wang, X. N., & Jiao, W. (2024). Self-control study of multi-omics in identification of microenvironment characteristics in urine of uric acid stone. Scientific Reports, 14(1), 25165.

[23]. Basiri, A., Tahvildari, A., Naji, M., Ziaeefar, P., & Kashi, A. H. (2025). Determination of the

kidney stone composition using infrared spectroscopy in Iran at a national referral center during 2019–2023. Asian Journal of Urology, 12(1), 72-78.

[24]. Zhang, J., Li, K., Chen, H., Hu, X., Guo, Z., Chen, S., ... & Chen, P. (2023). Retrospective analysis of urinary tract stone composition in a Chinese ethnic minority colony based on Fourier transform infrared spectroscopy. Scientific Reports, 13(1), 13453.

[25]. Acharya, A., Khanal, M., Maharjan, R., Gyawali, K., Khanal, K., Kshetri, M. B., ... & Lamichhane, H. P. (2024). Experimental FTIR characterization of kidney stones, DFT analysis of CaC2O4 and its interactions with lysozyme. BIBECHANA, 21(3), 311-320.

[26]. Tseregorodtseva, P. S., Budylin, G. S., Zlobina, N. V., Gevorkyan, Z. A., Filatova, D. A., Tsigura, D. A., ... & Shirshin, E. A. (2023, December). Multiwavelength Fluorescence and Diffuse Reflectance Spectroscopy for an In Situ Analysis of Kidney Stones. In Photonics (Vol. 10, No. 12, p. 1353). MDPI.

[27]. Boichenko, E., Paronnikov, M., & Kirsanov, D. (2023). Pilot Study on the Qualitative Analysis of Urinary Stones Using Near-Infrared Spectroscopy and Chemometrics. Engineering Proceedings, 48(1), 64.

[28]. Ozono, C., Hirasawa, I. and Kohori, F. (2017), Shape Change and Growth Behavior of Monosodium Urate Monohydrate in a Gout Model. Chem. Eng. Technol., 40: 1231 1234. 0.

[29]. Norazmi, N., Rasad, Z. A., Mohamad, M., & Manap, H. (2017), Uric acid detection using UV-Vis spectrometer. IOP Conf. Ser.: Mater. Sci. Eng 257(1), 012031.

[30]. Khalil, A. A. I., Gondal, M. A., Shemis, M., & Khan, I. S. (2015). Detection of carcinogenic metals in kidney stones using ultraviolet laser-induced breakdown spectroscopy. Applied optics, 54(8), 2123-2131.

[31]. Tsung-Jui Lin., Kai-Ting Yen., Chien-Fan Chen., Shuo-Ting Yan., Kuan-Wei Su., & Ya-Ling Chiang, Label-Free Uric Acid Estimation of Spot Urine Using Portable Device Based on UV Spectrophotometry, (2022), Sensors, 22, 3009.